2023 45th Annual International Conference of the IEEE Engineering in Medicine & Biology Society (EMBC) | 979-8-3503-2447-1/23/$31.00 ©2023 IEEE | DOI: 10.1109/EMBC40787.2023.10340812

Regularization parameter based on incomplete variables for X-ray luminescence computed tomography

Huangjian Yi, Zijian Tang, Ruigang Yang, Fengjun Zhao, Xin Cao, Lizhi Zhang, Xiaowei He and Yuqing Hou

***Abstract*—X-ray luminescence computed tomography (XLCT) is an emerging molecular imaging technique for biological application. However, it is still a challenge to get a stable and accurate solution of the reconstruction of XLCT. This paper presents a regularization parameter selection strategy based on incomplete variables frame for XLCT. A residual information, which is derived from Karush-Kuhn-Tucker (KKT) equivalent condition, is employed to determine the regularization parameter. This residual contains the relevant information about the solution norm and gradient norm, which improved the recovered results. Simulation and phantom experiments are designed to test the performance of the algorithm.**

***Clinical Relevance*— The results have not yet been used in clinical relevance currently, we believed that this strategy will facilitate the development of the preclinical applications in FMT.**

I. INTRODUCTION

X-ray luminescence computed tomography (XLCT) is a novel molecular imaging tool proposed in recent years [1-4]. It has the potential to trace specific molecular. In this imaging process, X-ray excites the phosphor nanoparticle (such as Lu, Eu, Ce, Pr, Nd, Sr) to produce visible or near infrared (NIR) luminescence light signals, which can be measured by charge coupled device (CCD) [5]. With a suitable mathematical model, one can reconstruct the spatial distribution of the phosphor nanoparticle from the measurement [3-5]. Compared to the regular optical molecular tomography, the main advantages of XLCT are the increased excitation depth in tissue and the elimination of tissue auto-fluorescence.

The narrow beam X-ray excitation technology known as XLCT is proposed by Xing *et. al.* [6]. To reduce the data acquisition time, a limited angle X-ray luminescence tomography reconstruction is carried out from limited-angles in narrow beam XLCT [7]. Chen *et. al.* developed a cone beam X-ray luminescence computed tomography (CB-XLCT) imaging system, which decreased the data acquisition time greatly by using a cone beam X-ray illumination [4]. Furthermore, Liu et. al. reconstructed the phosphor nanoparticle with single-view data by CB-XLCT imaging system, which does not need to rotate the imaged object to obtain multiple-view data [8]. Similar to FMT and BLT, the reconstruction of XLCT is an ill-posed problem [9]. In our previous work, a three-term conjugate gradient (TTCG) algorithm is proposed to seek for the effective information in each direction based on the incomplete variable truncated conjugate gradient (IVTCG) algorithm [10]. It improves the convergence speed of the algorithm and can still achieve the reconstruction accuracy of IVTCG algorithm. However, the regularization parameter is still based on experience settings. For Tikhonov regularization, the L-curve method is commonly used for automatic selection of the regularization parameter [11]. It has been applied to optical tomography [12, 13]. However, it would yield an overly-smoothed solution in diffusion optical tomography [13]. As an alternative to L-curve, the U-curve method has been developed and studied in fluorescence molecular tomography (FMT) [14, 15]. Furthermore, M. Chen et al have made comparative studies on L-curve and U-curve methods for dynamic fluorescence molecular tomography (DFMT) [16].

In this work, we developed an adaptive regularization strategy based on KKT equivalent condition residual (KECR) adjustment. A residual information, which contains the relevant information about the solution norm and gradient norm is used to select regularization parameter. We show the feasibility of the KECR method for simulation and phantom experiments in XLCT.

II. METHOD

In the X-ray luminescence computed tomography, X-rays emitted from the x-ray source traveled through the tissues to irradiate the nanophosphors, and the nanophosphors will emit visible or NIR light, as shown as follows [6]:

$$S(r) = \varepsilon X(r)\rho(r) \tag{1}$$

where $S(r)$ is the intensity of the emitted light, $X(r)$ is the X-ray intensity photon yield, $\rho(r)$ is the density of nanomaterial at the position of r, and ε is the photon yield. The energy distribution of X-ray in the tissues according to Beer-Lambert's law is expressed as follows [17]:

$$X(r) = X_0 \exp\left\{-\int_{r_0}^{r} \mu_t(\tau)d\tau\right\} \tag{2}$$

where $\mu_t(\tau)$ is the X-ray attenuation coefficient at τpoint, and $X_0$is the X-ray concentration at the initial position. $\boldsymbol{r_0}$ and r represent the initial and current position, respectively. The transmission of light in tissues with high scattering and low absorption can be modeled by the following diffusion equation (DE) [4, 18]:

$$-\nabla[D(r)\nabla\Phi(r)] + \mu_a(r)\Phi(r) = S(r), r \in \Omega \tag{3}$$

where Ω is the imaging region, $D(r)$ is the diffusion coefficient, and $\mu_a(r)$ is the absorption coefficient. ∇ is the gradient operator, $S(r)$ is the light source, $\Phi(r)$ is the light

* This study was funded by the National Natural Science Foundation of China (61906154, 61971350, 61901374), the Youth Innovation Team of Shaanxi Provincial Department of Education (21JP123). Key Research and Development Projects of Shaanxi Province under Grant (20209SF-036).

All authors are with the Xi'an Key Laboratory of Radiomics and Intelligent Perception, the School of Information Sciences and Technology, Northwest University, Xi'an, China (corresponding author to provide e-mail: yhj2014@nwu.edu.cn).

979-8-3503-2447-1/23/$31.00 ©2023 IEEE
Authorized licensed use limited to: FUDAN UNIVERSITY. Downloaded on December 19,2023 at 04:24:34 UTC from IEEE Xplore. Restrictions apply.

intensity at position r. The finite element method (FEM) is employed to solve Eq. (3) and the reconstruction problem can be transformed into the following equation [4, 18]:

$$AS = \Phi \tag{4}$$

where A is the system matrix of size $M * N$, $\Phi$is the photon flow rate, S is the internal energy density. Based on the compressed sensing theory and l_1 regularization, Eq. (4) is considered as:

$$\min_{S} \|AS - \Phi\|_2^2 + \tau\|S\|_1 \tag{5}$$

where τ is the regularization parameter.

Since the Eq. (5) is convex non-differentiable, we reformulate it as a convex quadratic function with non-negative constraints by the gradient projection method used in sparse reconstruction, which is a kind of large-scale function for compressed sensing. First, we introduce vectors u and v, and replace $\rho = u - v, u \geq 0, v \geq 0$. Eq. (5) becomes the following equation:

$$\min_{z} c^T z + \frac{1}{2} z^T B z = F(z) \tag{6}$$

where $z = [u \quad v]^T$, $c = \tau \mathbf{1}_{2N} + [-b \quad b]^T$, $\mathbf{1}_{2N} = [1,1,\cdots,1]^T$, $b = A^T\Phi$, and $B = \begin{bmatrix} A^TA & -A^TA \\ -A^TA & A^TA \end{bmatrix}$。

An adaptive regularization strategy based on KKT equivalent condition residual (KECR) adjustment is proposed. In the incomplete variable reconstruction framework [16], since the objective function is a convex function, the necessary and sufficient condition for the solution z^* to satisfy the optimal solution of Eq. (5) must satisfy the Karush-Kuhn-Tucker (KKT) condition, namely:

$$\nabla F(z^*) \geq 0, z^* \geq 0, \left(\nabla F(z^*)\right)^T z^* = 0, \nabla F(z^*) + z^* > 0 \tag{7}$$

Then:
$$min\{z^*, \nabla F(z^*)\} = 0 \tag{8}$$

Therefore, the necessary and sufficient condition for z^* to be the optimal solution of the equation is $w \triangleq \|min\{z^*, \nabla F(z^*)\}\|_2 = 0$. The residual information obtained by the KKT condition is considered as the termination condition for the iteration. The residual information also contains the relevant information about the solution norm and gradient norm. Compared to the L-curve, it is easier to calculate the residual information obtained by the KKT equivalent condition since it only needs one output variable.

In the L-curve method, the most important step is to obtain the data set about the solution norm and the residual norm. Based on the data, the L-curve can be fitted and the inflection point of the curve can be found. Unfortunately, it is difficult and time-consuming to realize this process in many applications. In the KECR, however, it does not need to obtain the final result under each regularization. And it only needs to adjust the size of the regularization parameter according to the residual information in the iterative process until the equilibrium condition is reached.

As shown in Fig. 1 (a), d_k is the descending direction, $normal$ is the normal vector normalized by l_1, $F(x_k)$ is the value of point x_k, and $\triangle_{min}$ is the minimized error. If the starting point is along the descending direction to find the extreme value, the next iteration point can only be obtained on the edge or inside of the regularization due to the regularization constraints.

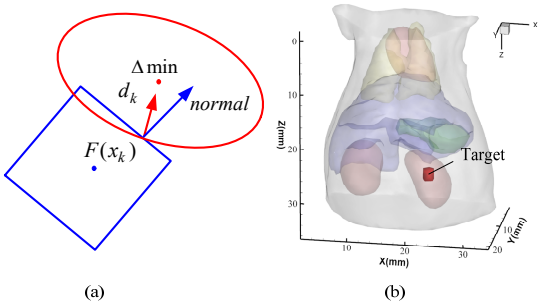

Fig. 1 (a) The optimal value solution graph after adding the regularization term. (b) The Position of single nanophosphor on 3D digital mouse.

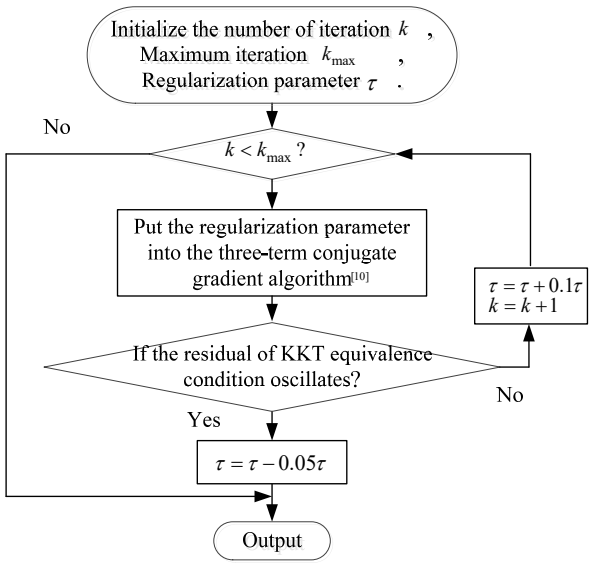

Fig. 2 The flowchart of the adaptive regularization parameter selection strategy based on the residual guidance.

Incorrect regularization parameters could result in the solution being deviated from the optimal solution. In general, too large regularization parameters could generate a strong constraint of regularization term. In this case, the residual error starts off in a state of oscillation and slow declines, which further causes an inaccurate result. Too small regularization parameters could make the variation of the residual in each iteration being close to the one with unconstrained condition. Due to the poor regularization constraint, the result has a large error and a slow convergence. In the L-curve method, the appropriate regularization parameters are obtained when the balance between the solution norm and the residual norm is good. Based on this idea, it's natural for us to find the balance relationship under the KKT equivalent condition to select the appropriate regularization parameter. Then, the KKT-equivalent conditional residual in the iterations shows oscillatory or slowly descending. At the balance of oscillation and slow decline, the regularization parameter is usually appropriate. Therefore, we use the residual under KKT-equivalent to balance the current regularization parameters, which is described as follows:

Authorized licensed use limited to: FUDAN UNIVERSITY. Downloaded on December 19,2023 at 04:24:34 UTC from IEEE Xplore. Restrictions apply.

$$\gamma = \|min\{z^*, \nabla F(z^*)\}\|_2 \quad (9)$$

A small value of the regularization parameter is given at the beginning. If γ has a decreasing convergence, it is generally considered that the constraint of the regularization term is not enough and the regularization parameter should be increased. If γ has an oscillation convergence, it is considered that the value of the regularization parameter is too large. It has to reduce the regularization parameter and the corresponding regularization parameter is selected as a well-posed one. The flow chart of the method is presented in Fig. 2.

The regularization parameters are selected by judging whether the equivalent conditional residuals oscillate in each iteration. And the plot demonstration of Eq. 9 is shown in Fig. 3. The red curve shows the residuals formed by the equivalent conditions of KKT decrease slowly when the regularized parameters are too small. The green one shows that the regularized parameter is too large, the residual error containing the gradient norm information will oscillate down.

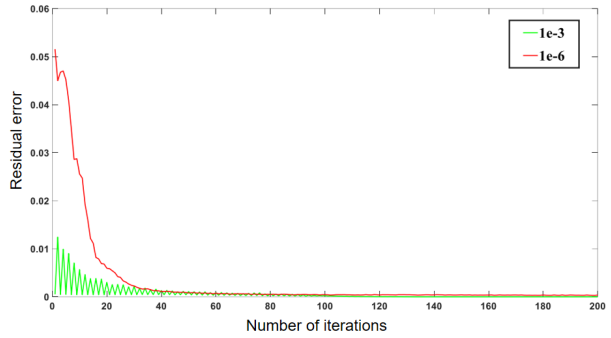

Fig. 3 Variations of residual with different regularization parameters

III. EXPERIMENTS

In order to study the feasibility of KECR, the commonly used L-curve and U-curve are considered as the comparison methods. Location error (LE), normalized root-mean-square error (NRMSE), and Dice coefficient (Dice) are used as indicators to evaluate the reconstruction accuracy, which could be found the detailed descriptions in [4, 10]. In general, a high-quality reconstructed image possesses LE, NRMSE being close to 0, and a high Dice value (0<Dice<1).

A. Numerical Simulation Experiments

The trunk part of a digital mouse is considered in this section. The body consists of six parts, muscle, heart, stomach, liver, kidneys and lung. In the case of a single target, the nanophosphor was a cylinder with a radius of 1mm and a height of 2mm, which was placed in the right kidney of the digital mouse with a central position of (23.0, 15.0, 26.0) mm, as shown in Fig. 1 (b). The forward grid contains 15562 nodes and 80984 tetrahedrons.

TABLE I. Regularization parameter provided by different selection strategies and their reconstruction results for single target

Algorithm	Regularization parameter	error	Location error(mm)	NRMSE	DICE
TTCG	1e-5	1e-5	1.07	0.106	0.28
TTCG+KECR	1.3e-5	1e-5	0.53	0.021	0.67
TTCG+L-curve	4.13e-5	1e-5	0.56	0.022	0.52
TTCG+U-curve	3.78e-5	1e-5	0.57	0.022	0.43

The initial regularization parameter is set to be 1e-5, which serves as a comparative test. The KECR strategy provided the regularization parameter by searching upward from the initial value. L-curve and U-curve are the regularization parameter values obtained at the inflection point and the lowest point of the curve after fitting the curve. All iteration termination error values are set to 1e-5. Table I and Fig. 4 showed the recovered results. When nothing was done with the regularization parameter the result is poor. Due to the existence of a large number of sparse artifacts, the DICE coefficient of reconstruction results is only 0.28, which is the lowest one of all. It is worth noting that the recovered results by the other three parameter selection strategies are similar according to LE and NRMSE, but the DICE coefficient of reconstruction results of KECR strategy reaches 0.67, which is better than the other two strategies. The black circles in Fig. 4 (b), (d), (f) and (h) represent the real position of the nanophosphor. It can be seen that the reconstruction results without using the parameter selection strategy have poor accuracy, as shown in Fig. 4 (a) and (b). The results by KECR strategy can cover the real target well from Fig. 4 (c). The regularization parameters selected by L-curve and U-curve can also provide high-precision results, but the reconstruction results of the two methods cannot completely cover the real target, as shown in Fig. 4 (e) and (g).

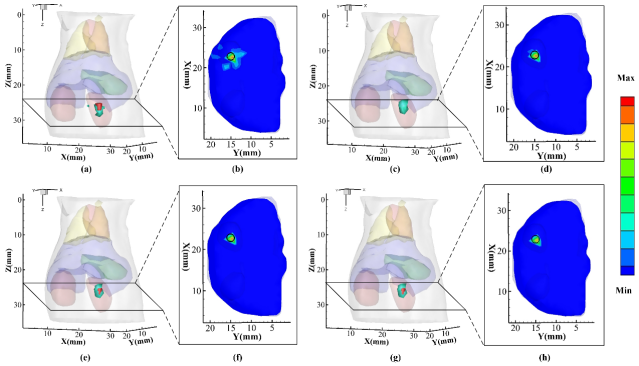

Fig. 4 Reconstruction results of different parameter selection strategies for single target. (a), (b) are TTCG reconstruction results. (c), (d) are TTCG+KECR reconstruction results. (e), (f) are TTCG+L-curve reconstruction results. (g), (h) are TTCG+U-curve reconstruction results.

B. Phantom Experiments

TABLE II. Regularization parameter provided by different selection strategies and their reconstruction results in phantom experiment

Algorithms	Regularization parameter	error	Location error(mm)	NRMSE	DICE
TTCG	1e-10	1e-5	1.35	0.036	0.12
TTCG+KECR	6.22e-4	1e-5	0.74	0.014	0.68
TTCG+L-curve	1.04e-5	1e-5	1.89	0.016	0.14
TTCG+U-curve	8.44e-7	1e-5	2.13	0.021	0.07

A cylinder with a radius of 10mm and a height of 20mm is utilized to simulate the real tissue. The cylinder is synthesized from polyformaldehyde. A small cylindrical light source is placed in the cylinder. The light source is composed of europium oxide and its position is (0.0, 7.5, 13.0) mm. The absorption and scattering coefficients are 0.025 mm^{-1} and 11.15 mm^{-1}. Fig. 5 (a) shows the phantom structure reconstructed by CT, which contains a europium oxide cylinder with a diameter of 2mm and a height of 2mm.

Authorized licensed use limited to: FUDAN UNIVERSITY. Downloaded on December 19,2023 at 04:24:34 UTC from IEEE Xplore. Restrictions apply.

As shown in Table Ⅱ, we set the initial regularization parameter as 1e-10 in the phantom experiment. The KECR strategy searches from the initial value and finally provides the regularization parameter of the equilibrium point. The regularization parameters of L-curve and U-curve are taken at inflection point and the lowest point respectively.

Fig. 5 shows the 3D view and 2D section view of the reconstruction results under different regularization parameter selection strategies. It can be seen that the algorithm using initial regularization parameters cannot obtain high-precision reconstruction results, with LE being greater than 1mm. The regularization parameters selected by KECR strategy can find the target with LE within 1mm, and the DICE coefficient is up to 0.68. The regularization parameters selected by L-curve and U-curve can provide the recovered results with LE being larger than 1.5mm. Therefore, the regularization parameters selected by KECR strategy can effectively make the reconstruction algorithm obtain high-precision result.

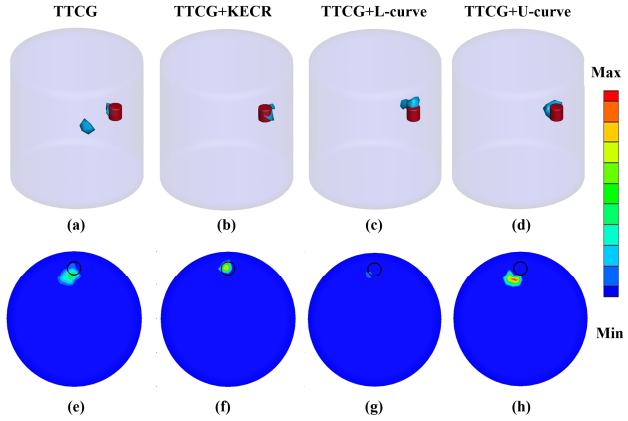

Fig.5 Reconstruction results of different parameter selection strategies in the phantom experiment. (a)-(d) are the parameter selection by TTCG, TTCG+KECR, TTCG+L-curve, TTCG+U-curve, respectively. (e)-(h) are the corresponding results at transverse views.

IV. Conclusion

In this paper, we have studied the residual correlation properties of KKT equivalent condition under the framework of solving incomplete variables. Then we proposed a regularization parameter selection strategy based on KKT equivalent condition residual. The equilibrium conditions in the KECR strategy are determined by the oscillation of the KKT equivalent condition residual in the iterative process. The regularization parameter is determined when the oscillation is changed. L-curve and U-curve methods were also employed.

In summary, the KECR strategy can provide an appropriate regularization parameter to obtain good results of TTCG algorithm. Without the frame of incomplete variables, the KECR strategy will become an invalid algorithm. So, it has a limited application compared with L-curve and U-curve methods. In the future, we will pay a great attention to the mixed residuals to find the optimal regularization parameters. It is necessary to explore a regularization parameter selection strategy with wide applicability.

References

[1] G. Pratx, C. M Carpenter, C. Sun and L. Xing, "X-ray luminescence computed tomography via selective excitation: a feasibility study," *IEEE Trans. Med. Imaging*, vol. 29, no. 12, pp. 1992-1999, 2010.

[2] X. Dai, K. Cheng, W. Zhao and L. Xing, "X-ray-induced shortwave infrared luminescence computed tomography," *Opt. Lett.*, vol. 44, no. 19, pp. 4769-4772, 2019.

[3] C. Li, K. Di, J. Bec, and S. R. Cherry, "X-ray luminescence optical tomography imaging: experimental studies," *Opt. Lett.*, vol. 38, no. 13, pp. 2339–2341, 2013.

[4] D. Chen, S. Zhu, X. Cao, F. Zhao, and J. Liang, "X-ray luminescence computed tomography imaging based on X-ray distribution model and adaptively split Bregman method," *Biomed. Opt. Express*, vol. 6, no. 7, pp. 2649-2663, 2015.

[5] H. Pu, P. Gao, J. Rong, W. Zhang, T. Liu, and H. Lu, "Spectral-resolved cone-beam x-ray luminescence computed tomography with principle component analysis," *Biomed. Opt. Express*, vol. 9, no. 6, pp. 2844-2858, 2018.

[6] G. Pratx, C. M. Carpenter, C. Sun, R. P. Rao, and L. Xing, "Tomographic molecular imaging of x-ray-excitable nanoparticles." *Opt. Lett.*, vol. 35, no. 20, pp. 3345-3347, 2010.

[7] C. M. Carpenter, G. Pratx, C. Sun and L. Xing, "Limited-angle x-ray luminescence tomography: methodology and feasibility study," *Phys. Med. Biology*, vol. 56, no. 12, pp. 3487-3502, 2011.

[8] X. Liu, H. Wang, M. Xu, S. Nie and H. Lu, "A wavelet-based single-view reconstruction approach for cone beam x-ray luminescence tomography imaging," *Biomed. Opt. Express*, vol. 5, no. 11, pp. 3848-3858, 2014.

[9] C. Darne, Y. Lu, E. M. Sevick-Muraca.,"Small animal fluorescence and bioluminescence tomography: a review of approaches, algorithms and technology update," *Phys. Med. Biology*, vol. 59, no. 1, pp. R1-R64, 2013.

[10] Y. Hou, Z. Tang, H. Yi, H. Guo, J. Yu, X. He, "Three-term conjugate gradient method for X-ray luminescence computed tomography," *J. Opt. Soc. Am. A*, vol. 38, no. 7, pp. 985-991, 2021.

[11] P. C. Hansen and D. P. Oleary, "The Use of the L-Curve in the Regularization of Discrete Iii-Posed Problems," *SIAM J. Sci. Comput.*, vol. 14, no. 6, pp. 1487-1503, 1993.

[12] T. Correia, A. Gibson, M. Schweiger, and J. Hebden, "Selection of regularization parameter for optical topography," *J. Biomed. Opt.*, vol. 14, no. 3, 2009.

[13] J. P. Culver, R. Choe, M. J. Holboke, L. Zubkov, T. Durduran, A. Slemp, V. Ntziachristos, B. Chance, and A. G. Yodh, "Three-dimensional diffuse optical tomography in the parallel plane transmission geometry: evaluation of a hybrid frequency domain/continuous wave clinical system for breast imaging," *Med. Phys.*, vol. 30, no. 2, pp. 235-247, 2003.

[14] D. Krawczyk-Stando and M. Rudnicki, "Regularization parameter selection in discrete ill-posed problems – The use of the U-curve," *Int. J. Appl. Math Comp.*, vol. 17, no. 2, pp. 157-164, 2007.

[15] J. Chamorro-Servent, J. Aguirre, J. Ripoll, J. J. Vaquero, and M. Desco, "Feasibility of U-curve method to select the regularization parameter for fluorescence diffuse optical tomography in phantom and small animal studies," *Opt. Express*, vol. 19, no. 12, pp. 11490-11506, 2011.

[16] M. Chen, H. Su, Y. Zhou, C. Cai, D. Zhang, and J. Luo, "Automatic selection of regularization parameters for dynamic fluorescence molecular tomography: a comparison of L-curve and U-curve methods," *Biomed. Opt. Express*, vol. 7, no. 12, pp. 5021-5041, 2019.

[17] I. Seferis, C. Michail, I. Valais, J. Zeler, P. Liaparinos, G. Fountos, N. Kalyvas, S. David, F. Stromatiad, E. Zycha, I. Kandarakisc, G. Panayiotakisb, "Imaging performance of a thin Lu2O3:Eu nanophosphor scintillating screen coupled to a high resolution CMOS sensor under X-ray radiographic conditions: comparison with Gd2O2S:Eu conventional phosphor screen," *Spie Medical Imaging*, vol. 9033, no., pp. 90333T-90333T-6, 2014.

[18] A. D. Klose, V. Ntziachristos, A. H. Hielscher, "The inverse source problem based on the radiative transfer equation in optical molecular imaging," *J. Biomed. Opt.*, vol. 202, no. 1, pp. 323-345 ,2005.

Authorized licensed use limited to: FUDAN UNIVERSITY. Downloaded on December 19,2023 at 04:24:34 UTC from IEEE Xplore. Restrictions apply.